A Goldilocks principle for modeling radial velocity noise

F. Feng[1]⋆, M. Tuomi[1], H. R. A. Jones[1], R. P. Butler[2] and S. Vogt[3]

[1] *Centre for Astrophysics Research, University of Hertfordshire, College Lane, AL10 9AB, Hatfield, UK*
[2] *Department of Terrestrial Magnetism, Carnegie Institute of Washington, Washington, DC 20015, USA*
[3] *UCO/Lick Observatory, Department of Astronomy and Astrophysics, University of California at Santa Cruz, Santa Cruz, CA 95064, USA*

16 June 2016

ABSTRACT

The doppler measurements of stars are diluted and distorted by stellar activity noise. Different choices of noise models and statistical methods have led to much controversy in the confirmation of exoplanet candidates obtained through analysing radial velocity data. To quantify the limitation of various models and methods, we compare different noise models and signal detection criteria for various simulated and real data sets in the Bayesian framework. According to our analyses, the white noise model tend to interpret noise as signal, leading to false positives. On the other hand, the red noise models are likely to interpret signal as noise, resulting in false negatives. We find that the Bayesian information criterion combined with a Bayes factor threshold of 150 can efficiently rule out false positives and confirm true detections. We further propose a Goldilocks principle aimed at modeling radial velocity noise to avoid too many false positives and too many false negatives. We propose that the noise model with $R_{\rm HK}$-dependent jitter is used in combination with the moving average model to detect planetary signals for M dwarfs. Our work may also shed light on the noise modeling for hotter stars, and provide a valid approach for finding similar principles in other disciplines.

Key words: methods: numerical; methods: statistical; methods: data analysis; Planetary Systems; techniques: radial velocities

1 INTRODUCTION

Almost all natural phenomena are studied by collecting and modeling data, comparing models and inferring model parameters. Since the data collection and reduction are usually standardised to remove bias and systematics, the results of data analyses are more influenced by the choice of models and inference methods than by data reduction[1].

Due to the limited explanation power of theories and models, natural phenomena are always left with inadequate or incomplete modeling. Thus our understanding of these unexplained variations (so-called "noise") significantly influences how well we can explain data particularly when noise levels are similar to those of variations. For example, the glacial-interglacial cycles over the Pleistocene era were probably caused by the orbital variations of the Earth through modulating the incoming solar radiation (Milankovitch 1930; Hays, Imbrie & Shackleton 1976). However, this theory is challenged by various authors (Hasselmann 1976; Pelletier & Turcotte 1997; Wunsch 2004) using stochastic processes to model the climate change.

In the case of detections of exoplanets in the doppler measure-

ments of stars, the activity induced radial velocity (RV) variations are called "excess noise" or "jitter", compared with the RV variations caused by Keplerian motions of planets (called "signals"). Jitter is typically correlated (or red) over various time scales (Baluev 2013), and is caused by various mechanisms such as instability of instruments, magnetic cycles, oscillation, rotation and granulation of stars (Dumusque et al. 2012). Jitter actually consists of unmodeled variations as well as pure noise. This jitter is poorly understood and modeled, leading to the problem of model incompleteness (Fischer et al. 2016). To separate jitter from planetary signals, many noise models are proposed based either on statistical properties of the RV time series (e.g., Baluev 2013) or on astrophysical studies of stellar variability (e.g. Rajpaul et al. 2015). The number of planetary candidates are sometimes greatly influenced by the choice of these noise models. For example, six planets have been claimed to orbit around GJ 581 (Vogt et al. 2010) based on data analysis applying the white noise model. However, Baluev (2013) could not confirm all of them using Gaussian process models. Similar controversies exist in the confirmation of exoplanets around GJ 667C using the white noise, moving average and Gaussian process models (Anglada-Escudé et al. 2013; Feroz & Hobson 2014). These controversies show that the more flexible the noise model is, the less planetary signals it can find. We will see this effect in the comparison of noise models.

Another factor that causes uncertainties in data analysis is the usage of different statistical methods. For example, many studies

---

⋆ E-mail: f.feng@herts.ac.uk or fengfabo@gmail.com
[1] Actually, data reduction is also a kind of modeling that converts the primary observations into secondary data such as catalogues. But the process is well understood in a theoretical sense.

claimed periodicities in the data of mass extinctions and terrestrial impact craters based on the periodogram or other frequentist approach (Alvarez & Muller 1984; Raup & Sepkoski 1984; Melott et al. 2012). But there seems to be no evidence for periodicities in the data based on the Bayesian inference (Bailer-Jones 2011; Feng & Bailer-Jones 2013, 2014). The tension caused by statistics also exists in the confirmation of planetary candidates even if the same noise model is used. For example, Tuomi (2011) only found four planets using Bayesian methods while Vogt et al. (2010) found six using the same radial velocity data set of GJ 581 and the same noise model but based on the periodogram. The solution to such controversies relies on the exploration of appropriate modeling and inference methods based on a better understanding of the mechanisms underlying certain phenomena and a proper choice of statistical tools.

Most data analysis of radial velocity data was seen based on frequentist methods, in particular, the Lomb-Scargle periodogram and adaptations of it, e.g. two dimensional Keplerian Lomb-Scargle periodogram (O'Toole et al. 2009). However, the periodogram assumes that the noise in the time series is not correlated and that there is only one periodic signal in the data. Despite this, it is misused to search for multiple periodic signals. For example, only one Keplerian component is used to model a superposition of several Keplerian signals. Both of these assumptions are problematic if the strength of signals is comparable with the noise level (Tuomi & Jenkins 2012; Fischer et al. 2016). Furthermore, the periodogram assumes periodicity in the data rather than testing it by comparing periodic models with other models. Thus periodogram, by definition, is biased in terms of model comparison. This is particularly true when the mechanisms responsible for certain phenomena are complex and poorly modeled (e. g. aperiodic and/or quasi-periodic phenomena).

Despite these problems, various periodograms are broadly employed to identify planetary signals in RV observations because they are easy to calculate. To test the significance of a signal, a selected false alarm probability (FAP) of a periodogram is commonly used as a detection threshold. This metric is equivalent to the *p*-value which is used to reject null hypotheses such as the white noise model. However, the choice of null hypothesis is always arbitrary, and thus makes FAP unable to properly estimate the significance of a signal. Considering these drawbacks, periodograms should be used cautiously particularly in cases when the signal to noise ratio is not high and the host star is perturbed by multiple planets (Cumming 2004; Ford & Gregory 2007).

To avoid the above problems of the periodogram, we need a statistical tool to compare models on the same footing rather than rejecting simple null hypothesis. If we know exactly the underlying physics of certain phenomena, there would be no need to compare different models. But this is often not the case for natural phenomena. Hence a proper way to account for model incompleteness, model complexity and uncertainties of models and data is crucial for robust data analyses. Fortunately, such inference problems can be properly dealt with in the Bayesian framework (e.g., Kass & Raftery 1995; Spiegelhalter et al. 2002; Gregory 2005; von Toussaint 2011). For example, Bayesian inference methods assess the overall plausibility of a model by calculating its likelihood averaged over its prior distribution. This approach naturally accounts for the model complexity and thus models can be compared properly.

In addition to an appropriate inference method, a modeling principle should be established through quantifying the limitations of stochastic and deterministic models. We do this for the RV data

of M dwarfs by comparing various noise models in the following steps. First, we generate artificial data sets using noise models and the Keplerian model. For these data sets, we compare noise models using various signal detection criteria. Then we select the best criterion which confirms most true detections and rejects most false positives. We further apply the criterion to compare models for the data sets with injected Keplerian signals. Based on the results, we quantify the limitations of various noise models and devise a framework of noise models to detect planetary signals.

Our aim is to provide a quantitative comparison between noise models used in the literature. We quantify the disadvantages and advantages of each noise model within the Bayesian framework. Various inference criteria are investigated for representative RV data sets. We also present a new principle to model stellar jitter and identify planetary signals.

This paper is structured as follows. We describe the Bayesian inference method and signal detection criteria in section 2. In section 3, we introduce the models of RV variations, and define their prior distributions. Then we compare various noise models and signal detection criteria for artificial data sets in section 4. In section 5, we introduce three RV data sets and inject planetary signals into them for model comparison. Finally, we discuss the results and conclude in section 6.

2   DATA ANALYSIS AND INFERENCE METHOD

2.1   Model comparison

The Bayesian model comparison relies on the Bayes theorem which is

$$P(M_i|D) = \frac{P(D|M_i)P(M_i)}{\sum_j P(D|M_j)}, \qquad (1)$$

where $P(M_i|D)$ is the *posterior* of model M_i for data D, $P(D|M_i)$ and $P(M_i)$ are the *evidence* (also called the integrated likelihood) and the *prior* of model M_i, and the denominator is a normalisation factor. Then the ratio of the posteriors of two models is

$$\frac{P(M_i|D)}{P(M_j|D)} = \frac{P(D|M_i)}{P(D|M_j)} \frac{P(M_i)}{P(M_j)}. \qquad (2)$$

If no model is favoured a priori, i.e. $P(M_i)/P(M_j) = 1$, the posterior ratio becomes

$$\frac{P(M_i|D)}{P(M_j|D)} = \frac{P(D|M_i)}{P(D|M_j)} \equiv \mathrm{BF}_{ij} , \qquad (3)$$

where BF_{ij} is the odds of evidences of model M_i and M_j, and is called *Bayes factor*. Following Kass & Raftery (1995), we interpret $\mathrm{BF}_{ij} > 150$ as a strong evidence for M_i and against M_j.

For model M with parameters $\boldsymbol{\theta}$, the evidence is

$$P(D|M) = \int_{\boldsymbol{\theta}} P(D|\boldsymbol{\theta}, M)P(\boldsymbol{\theta}|M)\mathrm{d}\boldsymbol{\theta} , \qquad (4)$$

where $\boldsymbol{\theta}$ is the parameter vector of model M, $P(\boldsymbol{\theta}|M)$ is the prior distribution of parameters, and $\mathcal{L}(\boldsymbol{\theta}) \equiv P(D|\boldsymbol{\theta}, M)$ is the *likelihood*. The evidence is actually the normalisation factor of the posterior distribution of model parameters,

$$P(\boldsymbol{\theta}|D, M) = \frac{P(D|\boldsymbol{\theta}, M)P(\boldsymbol{\theta}|M)}{P(D|M)} . \qquad (5)$$

In most cases, the evidence cannot be calculated analytically due to the complexity of the likelihood. Thus a Monte Carlo approach

is required either to sample the prior density $P(\boldsymbol{\theta}|M)$ (prior sampling) or to sample the posterior density $P(\boldsymbol{\theta}|D, M)$ (posterior sampling) or to sample both. The prior sampling is not appropriate for RV models because the posterior density always contains multiple modes in the period space related to planets and activity-induced variations. The modes are typically narrow that the prior samples may not resolve the posterior distribution properly. Considering these difficulties in prior sampling, we sample the posterior and calculate the Bayes factors using various estimators which will be introduced in section 2.3.

2.2 Posterior sampling

To sample the posterior density, we use an adaptive Metropolis-Hastings algorithm of Markov Chain Monte Carlo (MCMC) developed by Haario, Saksman & Tamminen (2001). This algorithm adjusts the step of the sampler to explore the posterior efficiently. Considering possible nonlinear correlation between parameters and a non-Gaussian posterior, we run adaptive Metropolis-Hastings algorithms to obtain posterior samples of $10^6 - 10^7$ for inference. We use the Gelman-Rubin criteria to judge whether a chain approximately converges to a stationary distribution (Gelman & Rubin 1992).

Specifically, we conduct the following steps to produce posterior samples. First, we run four chains in parallel, and drop out one half of each chain as "burn-in" part. Second, we estimate the so-called "potential scale reduction factor" ($\hat{R}$) by calculating the variance between and within the chains according to the Gelman-Rubin criteria. If $\hat{R}$ is less than 1.1, we combine these chains to provide a statistically representative posterior sample for inference. Third, we repeat the above two steps to generate chains with different tempering parameters. A chain is tempered if it is generated with a probability of move that is proportional to a power of the posterior ratio of proposed parameters and current parameters. Tempering is used to improve the dynamic properties of a chain to explore the whole parameter space efficiently. The chain without tempering is called "cold chain" while the tempered chain is called "hot chain". Considering that the optimal acceptance rate of a Metropolis-Hastings algorithm is around 0.234 under general conditions (Roberts et al. 1997), we select the hot chains with acceptance rate between 10% and 35%. Then we identify the potential signal based on the maximum a posteriori estimation, and use the corresponding parameters as the initial conditions of a cold chain. Finally, the cold chain provides a sample drawn from the posterior density of the model. For models without a Keplerian component, we run cold chains directly to obtain their unimodal posterior densities. Because we aim at comparing noise models rather than models with multiple Keplerian components, we only obtain samples for models with at most one planetary component.

2.3 Signal detection criteria

Given a statistically representative sample drawn from the posterior density, we move on to calculate the evidence using various methods. The integral in Eqn. (4) can be calculated by the "importance sampling" method (Kass & Raftery 1995), which generates samples from a density. For example, the harmonic mean (HM) estimator of the evidence is calculated by averaging the likelihood over samples approximately drawn from the posterior density. However, this estimator cannot converge efficiently due to the occasional occurrence of samples with very low likelihoods. To solve the convergence problem of HM, Tuomi & Jones (2012) introduce the

truncated posterior mixture (TPM) by drawing samples from different sections of a MCMC chain to avoid the divergence caused by low likelihood values. This method is easy to implement because it only uses the output of Metropolis-Hastings algorithms. But this method is biased if its free parameter λ is large (Tuomi & Jones 2012; Díaz et al. 2016). In addition to importance sampling methods, we introduce the one-block Metropolis-Hastings method developed by Chib & Jeliazkov (2001). The Chib's estimator (CHIB) is based on the calculation of the posterior of a single point using samples drawn from the posterior density and the proposal density of a Metropolis-Hastings sampler.

Although the evidence can be approximately calculated by the above methods, they have limitations in applications to complex problems due to unrealistic assumptions or computation inefficiency (see Friel & Wyse 2012 and Han & Carlin 2011 for a review). Considering these, we also introduce various information criteria which are easy to calculate and thus are frequently used by practitioners. We introduce three of them: the Akaike Information Criterion (AIC; Akaike (1974)), the Bayesian Information Criterion (BIC; Schwarz et al. (1978)) and the Deviance Information Criterion (DIC; Spiegelhalter et al. 2002). The AIC and DIC are criteria motivated from information theory while the BIC is derived in the Bayesian framework[2]. Considering that the sample size of RV data sets may be small, we use a revised version of AIC introduced by Hurvich & Tsai (1989). We write the three criteria as follows.

$$AIC \equiv -2\ln\mathcal{L}_{\max} + \frac{2k(k+1)}{N-k-1} \tag{6}$$

$$BIC \equiv -2\ln\mathcal{L}_{\max} + k\ln N \tag{7}$$

$$DIC \equiv D(\bar{\theta}) + 2p_D = \bar{D}(\theta) + p_D , \tag{8}$$

where $\mathcal{L}_{\max}$ is the maximum likelihood, k is the number of free parameters[3], N is the number of data points, the deviance $D(\boldsymbol{\theta}) = -2\ln\mathcal{L}(\boldsymbol{\theta})$ and the effective number of parameters $p_D = \bar{D} - D(\bar{\boldsymbol{\theta}})$. To compare the above information criteria with the Bayes factor estimators, we transform these information criteria into a Bayes factor like quantities [4]. It is straightforward to convert the BIC into a Bayes factor because Kass & Raftery (1995) argued that $e^{-\Delta BIC_{10}/2} \to BF_{10}$ when the sample size is large. Here we define $\Delta BIC_{10} = BIC_1 - BIC_0$. We also define Bayes factor using the relative likelihood derived from AIC, i.e. $BF_{10} = e^{-\Delta AIC_{10}/2}$, where $\Delta AIC_{10} = AIC_1 - AIC_0$. We then derive Bayes factor from DIC in the same fashion, since the DIC probably approaches the AIC when parameters are well constrained (Liddle 2007). Note that the transformations from AIC and DIC to Bayes factor are without theoretical foundation. Rather, it is used to transform the threshold of AIC or DIC to the threshold of Bayes factor, making AIC or DIC approximately suitable for Bayesian inference.

With the above evidence estimators and information criteria, we adopt the following diagnostics for the presence of a Keplerian signal.

---

[2] Although the BIC is derived using the Laplace approximation of a Gaussian likelihood distribution and the likelihood distribution in our case is always multimodal, we use it because the likelihood is always dominated by the Keplerian signal if there is, and the local distribution around the maximum is always Gaussian.

[3] We assume that a free parameter could be any variable in a model as in the case of linear models. Although a more complex definition of the parameter number could be helpful for nonlinear models, this is equivalent to changing the Bayes factor threshold which we will do in section 5.2 .

[4] To make the notation simple, we still use BF to name this quantity.

• The period P of the signal can be constrained from above and below in the posterior density. In other words, it converges to a stationary distribution.

• The amplitude K of the signal is significantly greater than zero. Specifically, the posterior of $K = 0$, i.e. $P(K = 0|D, M)$, is less than 1% [5].

• The evidence of a model with one Keplerian component should be at least 150 times higher than the evidence for the model without any Keplerian component, i.e. $BF_{10} > 150$ (Kass & Raftery 1995).

The above procedure is also used by Tuomi (2012) in combination with the moving average model which we will introduce in the following section.

3   MODELING RADIAL VELOCITY VARIATIONS

The measured doppler shifts of a star are generated by gravitational force from star-planet(s) interactions and stellar activity. The spectroscopic measurements of these doppler shifts yield RV data with instrument uncertainties and various activity indexes. To account for these factors, we model the data by combining Keplerian components and various noise components. In the following sections, we introduce the basic model which includes the white noise model and the Keplerian component. Then we add various noise components onto the basic model to build other models in such a way that the basic model is nested in the full model given all noise components.

3.1   White noise model

There is good evidence in the architectures of the Solar System and exoplanetary systems for orbital resonances playing some role (e.g., semi-major axes of resonant trans-Neptunian objects). However, the importance is limited over the typically time span of RV data (e.g., Batygin 2015), and so we make the simplifying assumption that planetary orbits are indenpendent of each other in a planetary system. Although we only consider at most one Keplerian signal in this work, we introduce a model of multiple Keplerian signals for general cases. We adopt the following basic model of RV variations,

$$
\begin{aligned}
\hat{v}_b(t_i, \boldsymbol{\theta}) &= \sum_{j=1}^{n} f_j(t_i) + a\, t_i + b + \sum_k c_k I_k \\
f_j(t_i) &= K_j[\cos(\omega_j + \nu_j(t_i)) + e_j \cos(\omega_j)] ,
\end{aligned} \quad (9)
$$

where K_j, ω, ν_j, e_j are the amplitude, the longitude of periastron, the true anomaly and the eccentricity for the jth planetary signal. The true anomaly ν is an implicit function of time, and depends on the orbital period P and the orbital phase at the reference time M_0. It can be calculated by solving the Kepler's equation. Thus the Keplerian component for each planet contains five free parameters: K, P, e, ω and M_0. In addition to the above parameters, we use two parameters, a and b, to model the acceleration caused either by a companion or by the long period activity cycles of the star and the reference velocity. We also use c_k to model the linear dependence of radial velocity on the activity index I_k. Specifically, we use I_F, I_B and I_R to denote the width of the spectral lines (FWHM),

bisector span (BIS) and the $log(R'hk)$ (R_{HK}), respectively. Note that these indexes are included into the model in a deterministic way. But they will be used in section 3.4 and 3.5 to model the jitter in a stochastic way .

The white noise model accounts for the excess noise through the likelihood function:

$$
\mathcal{L}(\boldsymbol{\theta}) \equiv P(D|\boldsymbol{\theta}, M_w) = \prod_i \frac{1}{\sqrt{2\pi(\sigma_i^2 + s_w^2)}} \exp\left[-\frac{(\hat{v}_b(t_i, \boldsymbol{\theta}) - v_i)^2}{2(\sigma_i^2 + s_w^2)}\right],
$$
(10)

where σ_i is the observational noise at time t_i, s_w is the constant amplitude of the white noise, and v_i is the observed RV at time t_i. The jitter depends on stellar activity levels which are partly measured by various shape indexes of spectrum such as FWHM and BIS and activity proxies such as the R_{HK} index. The noises caused by activity and instruments are typically correlated (Baluev 2013), and are too complex to be modeled deterministically. Thus a range of red noise models are proposed to remove correlated noises which may mimic Keplerian signals. In the following sections, we introduce two of them: the moving average and Gaussian process models.

3.2   Moving average

The moving average (MA) model is used to model the dependence of current noise on previous noise. The moving average of order q or MA(q) is

$$
\hat{v}(t_i) = \hat{v}_b(t_i) + \epsilon_{t_i} + \sum_{j=1}^{q} k(t_i, t_{i-j})\epsilon_{t_{i-j}}, \quad (11)
$$

where $k(t_i, t_{i-j})$ is the kernel used to weight the white noise at time t_{i-j}. We introduce two kernel functions, the Laplacian kernel

$$
k_L(t_i, t_{i-j}) = w_j \exp(-\beta|t_i - t_{i-j}|) \quad (12)
$$

and the squared exponential kernel

$$
k_{\text{se}}(t_i, t_{i-j}) = w_j \exp(-\beta(t_i - t_{i-j})^2/2) , \quad (13)
$$

where w_j is a positive number for white noise at t_{i-j}, and β is a free parameter.

According to Tuomi et al. (2013), MA(1) is the best moving average model which enable the detection of weak signals. In addition, this model seems to outperform other red noise models in recent RV Challenge (Dumusque et al. 2016) conducted by Xavier Dumusque [6]. Hereafter we will use moving average to denote MA(1) and use the Laplacian kernel if not mentioned otherwise.

3.3   Gaussian process

The Gaussian process (GP) is included in the RV model by adding non-diagonal parts to the covariance matrix of the likelihood function (see Eqn. 10) which is

$$
\mathcal{L}(\boldsymbol{\theta}) \equiv P(D|\boldsymbol{\theta}, M_{gp}) = \frac{1}{\sqrt{|2\pi\mathcal{C}|}} \exp\left[-\frac{1}{2}(\boldsymbol{v} - \hat{\boldsymbol{v}}_b)\mathcal{C}(\boldsymbol{v} - \hat{\boldsymbol{v}}_b)\right],
$$
(14)

where $\boldsymbol{v}$ is the observed RV sequence (i.e. $\{v_i\}$), $\hat{\boldsymbol{v}}_b$ is the RV model expressed by Eqn. (9) (i.e. $\{\hat{v}_b(t_i, \boldsymbol{\theta})\}$), and $\mathcal{C}$ is the covariance matrix. The covariance matrix is composed of diagonal and

---

[5] In reality, we fit a normal distribution to the posterior sample, and from the best fitted posterior density we determine $P(K = 0|D, M)$.

[6] The details of RV Challenge data sets and results can be found online at https://rv-challenge.wikispaces.com.

non-diagonal components. The former is related to the Gaussian measurement noise $\{\sigma_i\}$ and the excess white noise s_w, while the latter is determined by a kernel. To calculate the covariance matrix, we introduce three types of kernels: Laplacian (L), squared exponential (se) and quasi-periodic (qp) kernels, which are formulated as follows.

$$
\begin{aligned}
k_{\mathrm{L}}(t,t') &= s_r \exp(-|t-t'|/l)\,, \\
k_{\mathrm{se}}(t,t') &= s_r \exp\left[-\frac{(t-t')^2}{2l^2}\right]\,, \\
k_{\mathrm{qp}}(t,t') &= s_r \exp\left[-\frac{\sin^2(\pi(t-t')/P_q)}{2l_p^2} - \frac{(t-t')^2}{2l^2}\right] \quad (15)
\end{aligned}
$$

where s_r is the red noise amplitude, l, l_p and l_e are correlation time scales, and P_q is the period of the quasi-periodic kernel. The L kernel is used by Baluev (2013) and Feroz & Hobson (2014), while the se and qp kernels are advocated by Rajpaul et al. (2015) in their Gaussian process framework used to disentangle activity-induced variations from planetary signals. In the comparison of noise models, we will focus on the Laplacian kernel, and use the other kenels for sensitivity tests.

3.4 R_{HK}-dependent jitter

It is well known that the solar activity is determined by the magnetohydrodynamic turbulence in the atmosphere, and thus is difficult to be accurately predicted due to the chaotic nature of turbulence (Petrovay 2010). Like the Sun, stars also show complex activity-induced variations (Tobias, Weiss & Kirk 1995) which are partly recorded by activity indexes in doppler measurements. Therefore the relationship between RV variations and activity indexes are probably complex (Vanderburg et al. 2016), and a deterministic relationship may not be appropriate to model the activity-induced RV counterpart. As a result, the dependence of RV on indexes should be modeled statistically. For example, Díaz et al. (2016) have proposed a linear dependence of jitter on the R_{HK} index. We call this model "R_{HK}-dependent jitter" (RJ) which replace the s_w in Eqn. (10) with

$$
s(t_i) = s_w + \alpha I_R(t_i)\,. \quad (16)
$$

Although Díaz et al. (2016) used a truncated version of the linear function, we don't explore more versions because the R_{HK}-dependent jitter model is flexible and representative, and does not require a fine-tuned threshold to truncate the R_{HK} index. For RV data sets that do not have R_{HK} index, I_R denotes the activity index which is determined by measuring the flux at the Ca II H&K lines with respect to continuum.

3.5 Lagged R_{HK}-dependent jitter

The activity of a star is determined by the underlying complex and nonlinear dynamics. Thus the time series generated by stellar activity typically have long correlation time scale (Boffetta et al. 1999). In a nonlinear dynamical system, the time series of state variables are actually projected from the motion on the manifold of a set of states. According to Takens (1981) the non-linear state space of the dynamics could be reconstructed by using only the lagged time series of one variable, e.g. the R_{HK} index in our case. Thus the jitter in the RV variations can be modeled as a function of the lagged activity indexes. Considering that the R_{HK} index is more sensitive to stellar activity (Dumusque, Boisse & Santos 2014), we let the jitter

$s(t_i)$ depend on the previous and subsequent R_{HK} indexes. Then the jitter noise becomes

$$
\begin{aligned}
s(t_i) &= s_w + \alpha I_R(t_i) + f(t_i, t_{i-1}) I_R(t_{i-1}) + f(t_i, t_{i+1}) I_R(t_{i+1})) \\
f(t,t') &= \eta \exp(-\kappa|t-t'|),
\end{aligned} \quad (17)
$$

where η is the amplitude of the correlation between jitter, and κ is the inverse of the correlation time scale. Replacing the white noise jitter s_w in Eqn. (10) by the above R_{HK}-dependent jitter, we define the lagged RJ model or LRJ. Considering that the lagged R_{HK} may induce the RV counterpart in a deterministic way, we propose another version of lagged RJ which is

$$
\hat{v}(t_i) = \hat{v}_b(t_i) + f(t_i, t_{i-1}) I_R(t_{i-1}) + f(t_i, t_{i+1}) I_R(t_{i+1}). \quad (18)
$$

We call the stochastic version in Eqn. (17) LRJ(S) and the deterministic version in Eqn. (18) LRJ(R). They are more alike than different in terms of accounting for time lagged R_{HK}, and thus share the same name. In other words, the lagged R_{HK} of LRJ(S) is put into the denominator of the exponential term of the likelihood (Eqn. 10) while the LRJ(R) model contains the lagged R_{HK} in the numerator. For a simulated data set, only one LRJ version will be chosen according to the ability of each LRJ model in finding signals.

In addition to the above mentioned noise models, we combine them to build compound models to make the comparison more comprehensive. We combine moving average with R_{HK}-dependent jitter to make the MARJ model, and combine moving average with lagged RJ to make the MALRJ model. For models with and without one Keplerian component, we add 1 and 0 after the model name, respectively. For example, MA1 means the moving average model with one Keplerian component while MA0 means the moving average model without Keplerian component[7]

3.6 Prior distributions

As a necessary part in Bayesian inference, the prior distributions of parameters are explicitly given for all models in table 5. For the Keplerian component in the white noise model, we adopt a Jeffreys prior for the period with a range from one day to the time span of the RV data sets. Following Tuomi & Anglada-Escudé (2013) we adopt a Gaussian prior distribution over eccentricity, i.e. $P(e) \propto \mathcal{N}(0, \sigma_e)$ with $\sigma_e = 0.2$, to account for observed eccentricity distribution (Kipping 2013) [8]. We adopt a uniform prior for the amplitude K with a upper limit of twice the maximum absolute value of RV. This prior is set not only to speed up the convergence of the chain but also to account for the fact that the long period signal (longer than the RV time span) is already modeled as a linear trend in Eqn. (9). The jitter amplitude s follows a uniform distribution from 0 to the upper limit of the prior of K. This is also the range of R_{HK}-dependent jitter $s(t_i)$. To make the chain converge quickly, we scale the R_{HK} index such that it has zero mean and unit variance. For the same reason, we define the ratio of the upper boundary of the prior of K, $K_{\max}$, and the difference between the maximum and minimum of the index variation as the upper limit of the parameters for the dependence of RV on activity indexes, c_R, c_F and c_B. For the Gaussian process model, we find that the likelihood of the Gaussian process model is not sensitive to the time

---

[7] This is not to be mixed with q^{th} order moving average models denoted as MA(q), we only apply MA(1) model.

[8] Although Kipping (2013) recommend beta distribution, we adopt the Gaussian distribution which is simpler and also flexible enough to describe eccentricities.

scale l, and thus set a narrow boundary for its prior. For the quasi-periodic kernel, we adopt the priors used by Mortier et al. (2016).

4   MODEL COMPARISON FOR ARTIFICIAL DATA SETS

To ensure that a model is suitable for the data, it is important to test them using artificial data sets with known noise. Otherwise, the model or its prior may not be appropriate for certain applications (Fischer et al. 2016). We will do this with two types of simulated data sets, artificial (with artificial signals and noise) and injection (with artificial signals and real noise) data sets. Comparing all models for these data sets, we quantify the limitations of these models and form a signal detection strategy. Fitting different models to the artificial data sets, we report the signals and models recovered by testing models according to the diagnostics in section 2.3.

We generate artificial data sets using three time samples and corresponding measurement errors: the sample from the Keck measurements of GJ 515A which contains 282 data points and two subsamples which are generated by randomly drawing 100 time samples from the full sample of GJ 515A. We denote these three samples as "full", "sub1" and "sub2", respectively. Then we generate the RV values using three models: white noise with one Keplerian component (W1), moving average with one Keplerian component (MA1) and Gaussian process with one Keplerian component (GP1). We vary the period $P \in \{20, 40, 80\}$ days and the amplitude of constant jitter $s \in \{0.5, 1, 2\}$ m/s. The other parameters are fixed, such that $K = 1$ m/s, $e = 0.1$, $\omega = \pi/2$, $M_0 = \pi/2$, $a = -0.1\,\mathrm{m\,s^{-1}yr^{-1}}$, $b = 1$ m/s, $(w, \beta) = (0.9, 0.25\,\mathrm{day^{-1}})$ and $(s_r, l) = (1\,\mathrm{m/s}, 3\,\mathrm{day})$. The total number of these artificial data sets is 54. Then we analyze each data set with the W0, W1, MA0, MA1, GP0 and GP1 models, and apply the signal detection criteria (see section 2.3) to confirm/reject potential signals. The results are shown in table 2.

4.1   Comparing models

In table 2, we observe that the white noise model recovers signals better than the red noise models. However, the white noise model also detects more false positives because it interprets correlated noise as signal. It is a surprise that the moving average model does not recover itself for the full and sub2 data sets with $(P, K) = (40\,\mathrm{day}, 1\,\mathrm{m/s})$. That means the moving average model interprets both the moving average noise and part of the signal as correlated noise, leading to an underestimation of the significance of the true signal. This indicates that a red noise model may not successfully separate correlated noise from planetary signals.

We also find that the white noise and moving average models could be recovered through applying at least one Bayes factor estimator for 10 and 7 data sets, respectively. However, the Gaussian process model is recovered for only 3 data sets. Due to the flexibility of the Gaussian process model in fitting a data set, it overfits the noise and thus underfits the signal, leading to a lower evidence. This problem is also evident from the fact that the Gaussian process model does not recover any true signals while the white noise and moving average models recover 4 and 3, respectively, for the Gaussian process generated data sets.

We can see the above differences between the white noise and moving average and Gaussian process models from their posterior densities in figure 1. We calculate the posterior densities by binning the posterior samples over the period and choosing the maximum
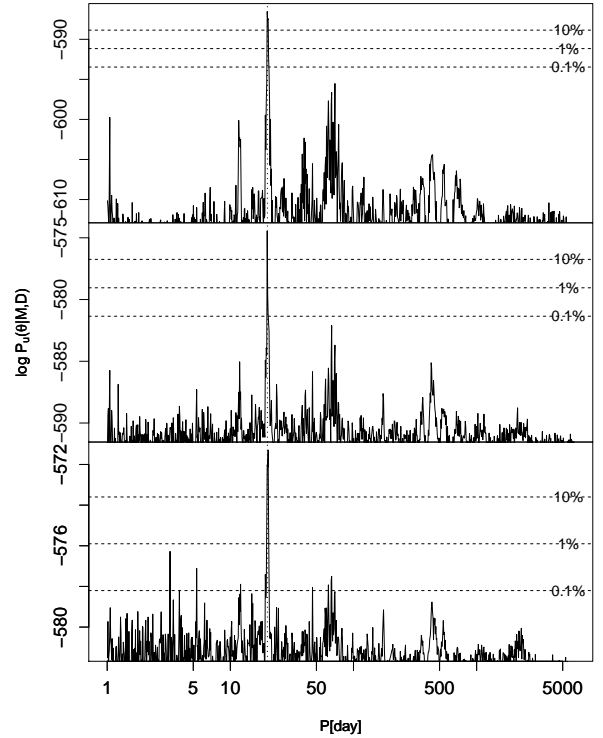

Figure 1. The unnormalised logarithm posterior density from the tempered chains for the white noise (upper), moving average (middle) and Gaussian process (lower) models for the full data set simulated using the Gaussian process model with $P = 20$day and $s = 1$m/s. To show the significance of signals in each panel, the 10%, 1% and 0.1% of the maximum a posterior is shown by dashed lines. The true period of the artificial signal is denoted by a vertical dotted line.

posterior in each bin as an approximation of the marginalised posterior. The significance of the signal can be inferred from the posterior difference between thresholds and the difference between the signal and noise. We find that the signal detected by the white noise model is more significant than those detected by red noise models, and the signal detected by the Gaussian process model is the weakest. We also observe that the broad peaks around 70 days are probably false positives. The red noise models reduce the significance of the false positives together with that of the signal. In other words, the cost of decreasing the false positive rate is increasing the false negative rate. We also notice that the peak around 1.05 day is probably an alias of the signal. But it is not as significant as the signal for all noise models. In particular, the red noise models seem to remove the alias efficiently due to their ability of modeling correlated noise over short time scales.

The performance of the models is also revealed by their maximum likelihoods shown in figure 2. We see that the planetary component can improve the maximum likelihood of white noise model more significantly than those of other models. This property of the white noise model is generic for all artificial data sets.

4.2   Choosing the optimum Bayes factor estimators

To further confirm the signal detections in table 2, we compare models with and without Keplerian component using the Bayes factor threshold BF > 150. We cannot calculate the Bayes factors of models which do not have any chains converged to the target signal

Table 1. The prior distributions of model parameters. The unit of c_1, c_2, c_3, α and η is m/s because the activity indexes are scaled before included in a model. The maximum and minimum time of the RV data are denoted by $t_{\max}$ and $t_{\min}$, respectively.

Parameter	Unit	Prior distribution	Minimum	Maximum
		Each Keplerian signal		
K_j	m/s	$1/(K_{\max} - K_{\min})$	0	$2|v|_{\max}$
P_j	day	$P_j^{-1}/\log(P_{\max}/P_{\min})$	1	$t_{\max} - t_{\min}$
e_j	—	$\mathcal{N}(0, 0.2)$	0	1
ω_j	rad	$1/(2\pi)$	0	2π
M_{0j}	rad	$1/(2\pi)$	0	2π
		Linear trend		
a	$\mathrm{m\,s^{-1}yr^{-1}}$	$1/(a_{\max} - a_{\min})$	$-365.24 K_{\max}/P_{\max}$	$365.24 K_{\max}/P_{\max}$
b	m/s	$1/(b_{\max} - b_{\min})$	$-K_{\max}$	$K_{\max}$
		Index dependence		
c_1	m/s	$1/(c_{1\max} - c_{1\min})$	$-c_{1\max}$	$K_{\max}/(I_{R\max} - I_{R\min})$
c_2	m/s	$1/(c_{2\max} - c_{2\min})$	$-c_{2\max}$	$K_{\max}/(I_{F\max} - I_{F\min})$
c_3	m/s	$1/(c_{3\max} - c_{3\min})$	$-c_{3\max}$	$K_{\max}/(I_{B\max} - I_{B\min})$
		Jitter		
s_w	m/s	$1/(s_{w\max} - s_{w\min})$	0	$K_{\max}$
α	m/s	$1/(\alpha_{\max} - \alpha_{\min})$	0	$K_{\max}/(I_{R\max} - I_{R\min})$
η	m/s	$1/(\eta_{\max} - \eta_{\min})$	0	$K_{\max}/(I_{R\max} - I_{R\min})$
κ	$\mathrm{yr^{-1}}$	$1/(\kappa_{\max} - \kappa_{\min})$	$365.24/(t_{\max} - t_{\min})$	1
		Moving average		
w	—	$1/(w_{\max} - w_{\min})$	-1	1
β	$\mathrm{day^{-1}}$	$1/(\beta_{\max} - \beta_{\min})$	$1/(t_{\max} - t_{\min})$	1
		Gaussian process		
s_r	m/s	$1/(s_{r\max} - s_{r\min})$	0	$K_{\max}$
l	day	$1/(l_{\max} - l_{\min})$	0.01	10
l_p	day	$l_p^{-1}/\log(l_{p\max}/l_{p\min})$	0.01	100
P_q	day	$1/(P_{q\max} - P_{q\min})$	1	100

Table 2. Comparison of noise models for artificial data sets. The Bayes factor of the one planet models (e.g. MA1) and corresponding zero planet models (e.g. MA0) are calculated for each data set. Without applying the threshold of $BF_{10} > 150$, the results of the test are denoted as A, B and C, which means that the signal is correctly recovered, not recovered (false negative) and falsely identified (false positive). The results obtained without and with applying the BIC-based BF threshold are written in normal and bold fonts, and corresponding detection numbers (denoted by N and n with subscripts) are reported without and with brackets, respectively. The flag A is underlined if the true model is recovered based on any estimator of the Bayes factor. The numbers of the data sets that have true models selected by any estimator and by the BIC is denoted by N_T and n_T, respectively.

| Sample	True model	W1			MA1			GP1		
	Test model	W1	MA1	GP1	W1	MA1	GP1	W1	MA1	GP1
full	$P = 20$day; $s = 1$m/s	**$\underline{A}$**	**A**	**A**	**A**	**$\underline{A}$**	**A**	**A**	**A**	B
	$P = 40$day; $s = 1$m/s	**$\underline{A}$**	**A**	**A**	**A**	B	**A**	**A**	**A**	A
	$P = 80$day; $s = 1$m/s	**$\underline{A}$**	**A**	**A**	**A**	**$\underline{A}$**	A	C	C	B
	$P = 20$day; $s = 2$m/s	**$\underline{A}$**	**A**	**A**	**A**	B	B	A	B	B
	$P = 40$day; $s = 2$m/s	B	B	B	**A**	B	B	**A**	**A**	B
	$P = 80$day; $s = 2$m/s	B	B	B	**A**	$\underline{A}$	A	B	B	B
sub1	$P = 20$day; $s = 0.5$m/s	C	B	B	**A**	**$\underline{A}$**	**A**	B	B	B
	$P = 40$day; $s = 0.5$m/s	$\underline{A}$	A	A	**A**	B	B	A	B	B
	$P = 80$day; $s = 0.5$m/s	$\underline{A}$	A	A	**A**	B	B	A	A	B
	$P = 20$day; $s = 1$m/s	B	B	B	B	B	B	**C**	**C**	**C**
	$P = 40$day; $s = 1$m/s	$\underline{A}$	B	B	B	B	B	A	A	$\underline{A}$
	$P = 80$day; $s = 1$m/s	B	B	B	B	B	B	B	B	B
sub2	$P = 20$day; $s = 0.5$m/s	$\underline{A}$	A	A	**A**	$\underline{A}$	A	B	B	B
	$P = 40$day; $s = 0.5$m/s	**$\underline{A}$**	**A**	**A**	**A**	$\underline{A}$	A	**A**	A	$\underline{A}$
	$P = 80$day; $s = 0.5$m/s	**$\underline{A}$**	**A**	**A**	**A**	**$\underline{A}$**	**A**	C	C	$\underline{A}$
	$P = 20$day; $s = 1$m/s	A	B	A	B	B	B	B	B	B
	$P = 40$day; $s = 1$m/s	B	B	B	**A**	B	**A**	B	B	B
	$P = 80$day; $s = 1$m/s	B	B	B	B	B	B	B	B	B
Numbers of flags for each model without (with) applying the threshold of BF > 150										
	$N_A(n_A)$	11(7)	9(6)	10(5)	13(10)	7(4)	9(6)	8(4)	6(3)	4(0)
	N_B	6	9	8	5	11	9	7	9	13
	$N_C(n_C)$	1(0)	0	0	0	0	0	3(2)	3(0)	1(0)
	$N_T(n_T)$	10(10)	—	—	—	7(3)	—	—	—	3(0)
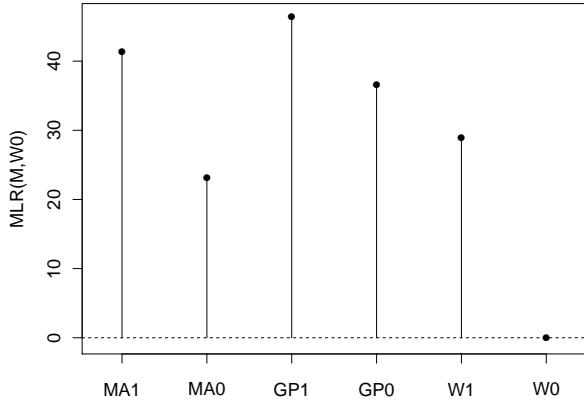
Figure 2. The maximum likelihood ratios (MLR) of various models and the W0 model for the full data set simulated by the Gaussian process model with $P = 20$day and $s = 1$m/s (the same data used in figure 1).

(denoted by flag "A" in table 2) due to a lack of statistically representative posterior samples. For data sets with recovered signals, we calculate the Bayes factor using the AIC, BIC, CHIB, DIC, HM and TPM estimators. To ensure the convergence of each method, we increase the size of the posterior sample gradually and calculate the Bayes factor for each sample size. Since the DIC cannot converge properly due to the asymmetry and multimodes of the posterior density, we only show the results for other estimators in figure 3. We find that the HM and TPM estimators give similar results since the HM is just a special case of the TPM (Tuomi & Jones 2012). However, neither of them converge very well due to the occasional occurrence of samples with very low likelihoods. The Bayes factor estimated by AIC is always higher than that estimated by the BIC and CHIB. We also see these differences from the Bayes factors calculated using the full posterior sample in figure 4. For models with one Keplerian component, we find that the DIC always estimate much higher Bayes factors while the BIC and CHIB estimate the lowest Bayes factors. However, for models without any Keplerian component, all methods give simliar Bayes factors, which justifies the usage of each method in the cases of unimodal posterior densities. We further investigate all data sets, and find that the Bayes factors estimated by AIC, HM and TPM are comparable, and the BIC and CHIB estimators always give similar results.

We then test the significance of signals using the Bayes factor threshold of 150. For each estimator of the Bayes factor, we apply the threshold to confirm recovered signals (denoted by " A"), false positives (denoted by " C") and recovered models (denoted by " T"). The ratios of confirmed and total number of them for all data sets[9] are used to characterize the ability of estimators combined with the Bayes factor threshold in confirming true signals and noise properties. The results for all estimators are reported in table 3.

In this table, we find that the DIC is not appropriate for confirming detections because it cannot rule out any false positive. On the contrary, the CHIB estimator is able to get rid of almost all false positives, but can only confirm 47% true detections. An appropriate choice is the AIC which could rule out about one quarter of the false positives, and confirm 96% of the true detections. Although

---

[9] To keep the notation simple, we continue to use N and n with subscripts to denote them (see table 2).
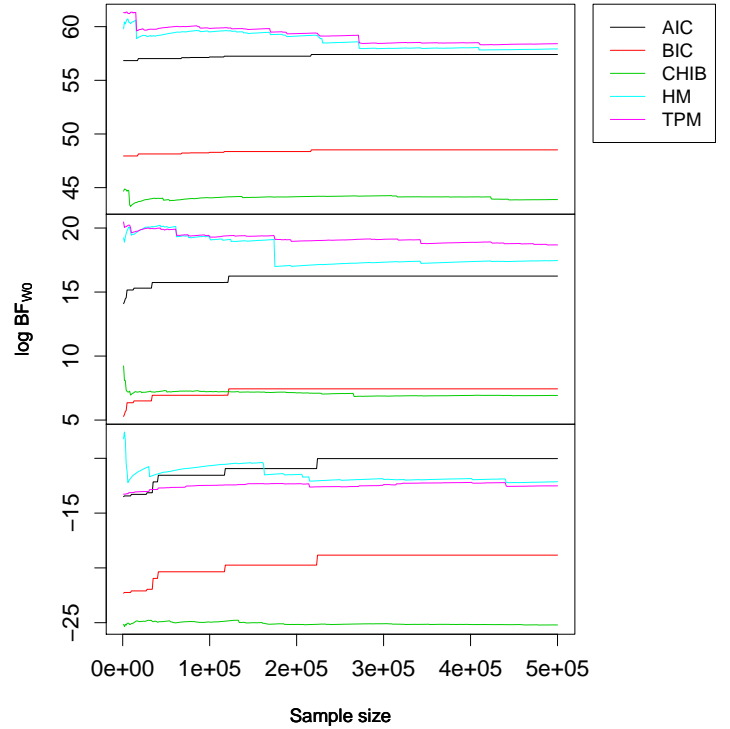

Figure 3. The convergence of Bayes factor estimators for the artificial data set generated by the moving average model with $P = 80$day and $s = 1$m/s. The upper, middle and bottom panels show the logarithm Bayes factors of W1, MA1, GP1, with respect to W0, respectively. The TPM estimator of Bayes factor is calculated with $\lambda = 10^{-4}$ as recommended by Tuomi & Jenkins (2012).
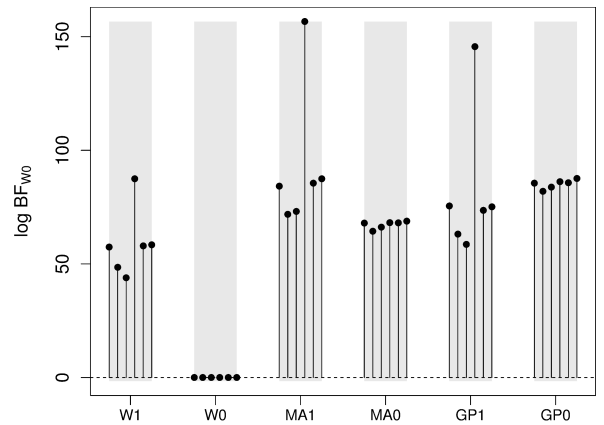

Figure 4. The Bayes factors estimated by various methods. The heights of the lines within each gray bar represent the Bayes factors of a certain model with respect to W0 estimated by AIC, BIC, CHIB, DIC, HM and TPM from left to right.

Table 3. The ratios used to characterise estimators. The notations are similar to those in table 2.

	AIC	BIC	CHIB	DIC	HM	TPM
n_A/N_A	0.96	0.58	0.47	1.0	0.90	0.90
n_C/N_C	0.75	0.25	0.13	1.0	0.88	0.88
n_T/N_T	0.75	0.65	0.60	0.40	0.70	0.50

the AIC is not a Bayesian criterion, we regard the AIC combined with a threshold as a practical tool to confirm detections. In the case of exoplanet detection, avoiding false positives is more important than avoiding false negatives. Such requirements can be satisfied by the BIC which rules out 75% false positives and confirms 58% true detections. In addition, the BIC recovers 75% true models while the CHIB method recovers 60%, justifying our choice of the BIC rather than the CHIB estimator to rule out false positives. Although the HM and TPM estimators confirm most true detections, they have convergence problems as we have mentioned (see figure 3).

In summary, the white noise model is able to detect weak signals efficiently while the Gaussian process are so flexible that signals are interpreted as correlated noise. The performance of the moving average model is somewhere between the performance of Gaussian process and white noise models. Moreover, most false positives could be ruled out by the BIC-estimated Bayes factor threshold of 150.

5 MODEL COMPARISON FOR INJECTION DATA SETS

In the above section, we have analysed the artificial data sets with known noises and signals. To make our analysis more general, we apply the same analysis method to data sets with known signals but with noises from real data. We adopt three data sets, the HARPS measurements of GJ 1 (44 epochs) and GJ 361 (101 epochs), and the Keck measurements of GJ 445 (64 epochs). For each data set, we use the RVs, measurement errors and activity indexes of $R_{\rm HK}$. We also consider the RV dependence on the FWHM and BIS index (see Eqn. 9) if they are available. Considering that the data of GJ 445 is not published before, we show it in the appendix. We introduce the three targets in the following section.

5.1 Radial velocity data

Most nearby stars now have precision radial velocities recorded for them. As of 2016 April the ESO archive for the HARPS instrument finds over 7000 different targets although most only have a few epochs some objects have large numbers, e.g., nearly 20,000 for alpha Centauri B. We focus our attention on radial velocity data for nearby M dwarfs. We choose these targets because they appear to have relatively lower activity noise. We have attempted to focus on targets which have reasonable sampling, good precision and for which there is enough radial velocity data to make detections but where there is not a strong known signal. We have drawn these from the sample of Tuomi et al. (2016) and specifically choose to study data from both HARPS (Mayor et al. 2003) and HIRES (Vogt et al. 1994). These are two of the pre-eminent radial velocity instruments whose design, calibration and processing can be considered both reliable and independent.

GJ 1 is a metal-poor (e.g., [Fe/H]=-0.45; Neves et al. 2012) M2 dwarf at a distance of 4.5 pc (van Leeuwen 2007) without any reported planetary companions (e.g. Zechmeister, Kürster & Endl 2009). Suárez Mascareño et al. (2015) find that it has a rotation period of 60.1 ± 5.7 d based on spectral activity indexes. Analysis of the ASAS photometric data (Pojmanski 2002) does not confirm this rotation period (Tuomi et al. 2016) though there are relatively modest 42 photometric data points spanning less than a year. We consider the 44 HARPS epochs which we have extracted from the ESO archive.

GJ 445 is a metal-poor (e.g., [Fe/H]=-0.30; Neves et al. 2012) M4 dwarf at a distance of 5.4 pc (van Leeuwen 2007) without any

reported planetary companions or rotational signals. Here we consider 64 epochs of Keck data.

GJ 361 is a slightly metal-poor (e.g., [Fe/H]=-0.11; Neves et al. 2012) M1.5 dwarf at 11 pc (van Leeuwen 2007). Tuomi et al. (2016) find a low amplitude signal (3.82m/s) with a period of 28.9 d which is removed from the data. Tuomi et al. (2016) do not find any evidence for significant periodicities in 241 ASAS V-band photometric observations of the star spanning 2,298 days. We utilise 101 epochs of HARPS radial velocity data.

To extract the noise from the GJ 361 data set, we analyze the data of GJ 361 with the moving model and identify the signal, and subtract the signal from the data set. This subtracted version is called "GJ361 subtracted". To ensure that no significant signal exist in the GJ 1, GJ 445 and GJ 361 subtracted data sets, we fit all models in section 3 to them and do not find any significant signal which satisfies the signal detection criteria. Fitting the W0 model to all data sets, we obtain the posterior of jitter-induced white noise s_w, and use the mean value as a reference point for choosing the amplitudes of injected Keplerian signals.

5.2 Recovering signals

To inject signals, we vary the amplitude and period of the Keplerian component and keep other parameters fixed. The amplitude of a signal is varied in such a way that the signal strength is lower, comparable or higher than the jitter level. We adopt $P \in \{20, 40, 80\}$ day for all data sets, $K \in \{1, 2, 4\}$ m/s for GJ 1 and GJ 361, and $K \in \{4, 6, 8\}$ m/s for GJ 445. The other Keplerian parameters are set $e = 0.1$, $\omega = \pi/2$, $M_0 = \pi/2$. Finally, we fit all noise models with and without planet to the injection data sets, and report the detections confirmed by the signal detection criteria in table 4.

As seen from table 4, no strong signals are found by any noise model, although the W1, RJ1 and LRJ1 models seem to identify weak signals which fail to pass the Bayes factor threshold. The table shows that the LRJ1 model detects the most signals without applying the BIC-estimated Bayes factor threshold ($\text{BF}_{10} > 150$) while the W1 and RJ1 models find the most signals once applying the threshold. On the contrary, red noise models only recover less than half of the injected signals and even less if applying the Bayes factor threshold, implying that they are much more conservative and prone to false negatives. However, if without applying the Bayes factor threshold, the moving average model can recover 13 signals. As a red noise model, moving average is not as flexible as Gaussian process, and thus is able to identify more signals. In addition, most true signals recovered by the W1, RJ1 and LRJ1 models are also strong in the posterior densities of the moving average model, although they may not satisfy the detection criteria. On the contrary, the false positives are never strong in the posterior distributions of moving average. Hence the moving average model can be used to confirm true detections and reject false ones.

To ensure that the results are not sensitive to the choice of kernels, we adopt the squared exponential kernel for the moving average models (see Eqn. 13), the squared exponential and quasi-periodic kernels for the Gaussian process models (see Eqn. 15). We fit the red noise models with these new kernels to the GJ1 data set with $(P, K) = (20 \text{ day}, 2 \text{ m/s})$, the GJ445 data set with $(P, K) = (80 \text{ day}, 8 \text{ m/s})$, and the GJ361 subtracted data set with $(P, K) = (80 \text{ day}, 2 \text{ m/s})$. For all these three data sets, we don't find any statistically significant improvement by changing kernels.

As we have mentioned in section 4, the red noise models interprets signals as noise, and thus adding a Keplerian component

Table 4. Model comparison for RV data sets without and with injected signals. We use the LRJ(S) and MALRJ(S) models to fit the GJ1 data set, and apply the LRJ(R) and MALRJ(R) models to fit the other data sets. The meanings of A, B and C are described in table 2.

data set	injected signal	MA1	GP1	W1	RJ1	LRJ1	MARJ1	MALRJ1
	—	B	B	B	B	B	B	B
	P= 20 day, K= 1 m/s	B	B	B	B	B	B	B
	P= 20 day, K= 2 m/s	B	B	**A**	**A**	A	A	A
	P= 20 day, K= 4 m/s	**A**	**A**	**A**	**A**	**A**	**A**	**A**
GJ1	P= 40 day, K= 1 m/s	B	B	C	B	B	B	B
	P= 40 day, K= 2 m/s	A	B	**A**	**A**	A	A	**A**
	P= 40 day, K= 4 m/s	**A**	**A**	**A**	**A**	**A**	**A**	**A**
	P= 80 day, K= 1 m/s	B	B	C	B	C	B	B
	P= 80 day, K= 2 m/s	A	B	**A**	**A**	A	A	A
	P= 80 day, K= 4 m/s	**A**	**A**	**A**	**A**	**A**	**A**	**A**
	—	B	B	C	B	B	B	B
	P= 20 day, K= 4 m/s	B	B	B	B	B	B	B
	P= 20 day, K= 6 m/s	B	B	C	C	A	B	B
	P= 20 day, K= 8 m/s	**A**	**A**	**A**	**A**	**A**	**A**	**A**
GJ445	P= 40 day, K= 4 m/s	A	B	**C**	B	**A**	B	A
	P= 40 day, K= 6 m/s	A	B	**A**	**A**	C	**A**	**A**
	P= 40 day, K= 8 m/s	A	**A**	**A**	**A**	**A**	**A**	**A**
	P= 80 day, K= 4 m/s	B	B	**C**	C	B	B	B
	P= 80 day, K= 6 m/s	B	B	B	B	B	B	B
	P= 80 day, K= 8 m/s	B	B	**A**	**A**	**A**	B	B
	—	B	B	C	C	C	B	B
	P= 20 day, K= 1 m/s	B	B	B	B	B	B	B
	P= 20 day, K= 2 m/s	B	B	B	B	B	B	B
	P= 20 day, K= 4 m/s	**A**	**A**	**A**	**A**	**A**	**A**	**A**
GJ361 subtracted	P= 40 day, K= 1 m/s	B	B	C	B	C	B	B
	P= 40 day, K= 2 m/s	**A**	**A**	**A**	**A**	**A**	A	A
	P= 40 day, K= 4 m/s	**A**	**A**	**A**	**A**	**A**	**A**	**A**
	P= 80 day, K= 1 m/s	B	B	B	C	B	B	B
	P= 80 day, K= 2 m/s	B	B	**A**	**A**	A	B	A
	P= 80 day, K= 4 m/s	**A**	**A**	**A**	**A**	**A**	**A**	**A**
Numbers of flags for each model without (with) applying the threshold of BF > 150								
	$N_A(n_A)$	13(8)	9(7)	15(15)	15(15)	16(14)	13(9)	15(9)
	N_B	17	21	7	11	10	17	15
	$N_C(n_C)$	0	0	8(2)	4(0)	4(0)	0	0

to a red noise model would not improve the likelihood as much as the W1 model does. This is evident from the comparison of the maximum likelihoods of all models in figure 5. We observe that the likelihoods of W1, RJ1 and LRJ1 are much higher than those of W0, RJ0 and LRJ0, indicating the necessity of adding one Keplerian component into the noise model. On the contrary, the Keplerian component does not significantly improve the likelihoods of the red noise models, in particular the Gaussian process model.

Among the W1, RJ1 and LRJ1 models, the W1 model give similar results as the RJ1 and LRJ1 models, although RJ1 and LRJ1 can model a few data sets slightly better due to adjusting extra free parameters. The LRJ1 model is favoured by the GJ445 data sets with $(P, K) =$(20 day, 6 m/s) and (40 day, 4 m/s). For the latter one, we show the posterior distribution of parameters α, η and κ of LRJ1 in figure 6. We observe that the white noise s_w dominates the total noise while the index dependent noises is consistent with zero. For all the other data sets, we don't find strong dependence of noise on the RHS index either. Despite this, the RJ1 and LRJ1 models give fewer false positives than the white noise model does, indicating a weak dependence of jitter on the RHS index. Furthermore, the false positives detected by RJ1 and LRJ1 failed to pass the Bayes factor threshold. This is not caused by the Bayesian penalization of model complexity because the Bayes factor of RJ1 (or LRJ1) and RJ0 (or LRJ0) do not depend on the number of parameters of the RJ (or LRJ) model. To test this further, we vary the

Bayes factor threshold to see whether there is an optimal threshold which can reject more false positives and keep all true detections. But we failed to find such a value. For example, we increase the Bayes factor threshold to be 200, and apply this new threshold to test the signals detected by the white noise model. We find that the false positives for the GJ445 data set with $(P, K) = (40$ day, 4 m/s) cannot be ruled out, and the true signal in the GJ1 data set with $(P, K) = (20$ day, 2 m/s) is rejected. It means that we cannot confirm all true signals recovered by the white noise model and reject false positives simultaneously by adjusting the Bayes factor threshold. Considering these problems of the white noise model and the complexity of the LRJ models, we recommend the R_{HK}-dependent jitter to model the excess noise in RV observations.

Considering the limitations of different noise models, we set up a rule for modeling RV noise and selecting signals in order to avoid as many false positives and negatives as possible. We call this rule "Goldilocks principle". Specifically, we suggest combining the white noise model and the R_{HK}-dependent jitter with the moving average model in the following way to confirm detections. First, we apply the three criteria introduced in section 2.3 to confirm a signal detected by the model of R_{HK}-dependent jitter. Then the signal is further confirmed if it is also strong and unique (without local maxima exceeding the 10% threshold, see figure 1) in the posterior distribution of the moving average model. Finally, the signal is confirmed as a planet if it is not found to be strong in the posterior
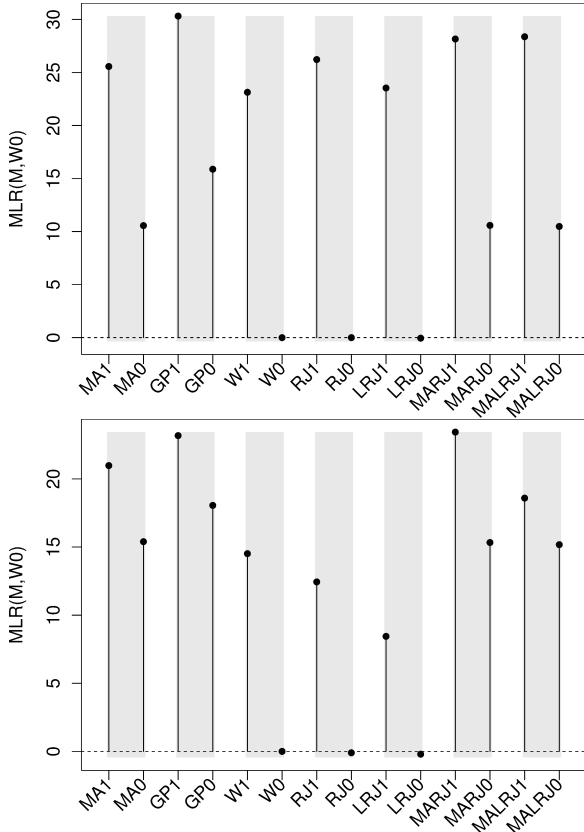
Figure 5. The maximum likelihood ratio (MLR) of noise models and the W0 model for the GJ445 data set with $P = 40\,\mathrm{day}$ and $K = 8\,\mathrm{m/s}$ and the GJ361 subtracted data sets with $P = 80\,\mathrm{day}$ and $K = 2\,\mathrm{m/s}$. Each grey bar encloses the MLRs for one noise model with and without planetary component.

distributions of the white noise model (with zero eccentricity) for the activity indexes to avoid detecting activity-induced false positives that have a different phase in the RVs and activity indexes.

6 DISCUSSIONS AND CONCLUSIONS

This work aims at comparing various noise models and inference criteria for detecting weak signals in radial velocity data sets. We define different noise models and introduce estimators of Bayes factor to analyse artificial data sets. We find that the white noise model is better than red noise models in detecting true signals. However, the white noise model tends to interpret correlated noise as a signal, and thus detect false positives. On the contrary, the red noise models, particularly the Gaussian process, usually interprets the signal as noise, at least partially, leading to false negatives. This is also the reason why the Gaussian process model is not favored even by the Gaussian process generated data sets (see table 2). This challenges the view that a simultaneous modeling of noise and signal components in data would not result in overfitting or underfitting problems (e.g. Foreman-Mackey et al. 2015). The solution of the problem is not only to perform modeling in the Bayesian framework but also to properly model noise and signal according to a Goldilocks principle which could be obtained for each specific scientific question.

Comparing various Bayes factor estimators, we find that the BIC estimation of Bayes factor combined with a Bayes factor

threshold of 150 can reject most false positives while other criteria either confirm more false positives or reject a large proportion of true detections. In addition, the truncated posterior mixture, harmonic mean and Deviance Information Criterion estimators do not converge properly. Meanwhile the Akaike Information Criterion and Chib's estimators penalize the one planet models too little and too much, leading to false positives and negatives, respectively. Given that all estimators of Bayes factors have short-comings (Ford & Gregory 2007), we adopt the BIC for practical reasons.

We have applied the BIC-based signal detection threshold to analyze data sets with injected signals. We have simulated 27 data sets by injecting signals with various periods and amplitudes into the HARPS measurements of GJ1 and GJ361 and the Keck observations of GJ445. We find that the white noise model and the (lagged) R_{HK}-dependent jitter models recover most injected signals. However, the Bayes factor threshold cannot reject all false positives found by the while noise model. Increasing the threshold cannot rule out all false positives and confirm all true detections simultaneously. On the contrary, the Bayes factor threshold successfully reject all false positives detected by the R_{HK}-dependent noise models, although the dependence of jitter on the R_{HK} is weak probably due to the low activity level of our targets. To make the planet detection conservative, we suggest to form a noise model framework by combining the R_{HK}-dependent noise model (RJ) and the moving average model. Since most planet hosts are M dwarfs, our conclusions on modeling the RV noise of M dwarfs are probably generic for exoplanet detections and so this work may also shed light on the noise modeling for hotter stars.

We also test the sensitivity of the evidences for red noise models to their kernels, and don't find any significant improvement for the test cases analysed here. Since the injection data sets are from different instruments and with different sizes, our quantification of the limitations of various noise models are probably generic for detecting planets in RV observations. Our results indicate that flexible noise models such as Gaussian processes may underestimate the number of Keplerian signals. This is supported by Tuomi et al. (2013)'s choice of first order moving average model to reduce jitter rather than higher order moving average models. In addition, the Tuomi et al. group "won" the RV Challenge using the moving average model while other groups failed to recover as many signals using more flexible models. This is consistent with our findings that the usage of flexible noise models tend to result in false negatives when the models do not correctly reflect the underlying physics of stellar activity.

This difference between noise models is also evident from the controversy over the validation of the number of planets, where red noise models find less signals than other models, e.g. GJ 581 and GJ 667C discussed in the introduction section. These controversies are consistent with our conclusion that red noise models lead to false negatives while the white (or R_{HK}-dependent) noise model lead to false positives. To avoid both, we define a Goldilocks principle by combining the R_{HK}-dependent noise model with the moving average model and a BIC-based signal detection criterion. This principle also provides a clue for noise modeling in other fields. For example, stochastic models may not be appropriate for modeling the glacial-interglacial cycles over the Pleistocene because they tend to give false negatives. This can be investigated through injecting Earth's orbital variations into noisy climate data and recovering them using stochastic noise models in combination with orbital models. Another example is the detection of periodic signals in quasar light curves. The optical variability of quasars could be caused by random processes, rotations of binary black holes,
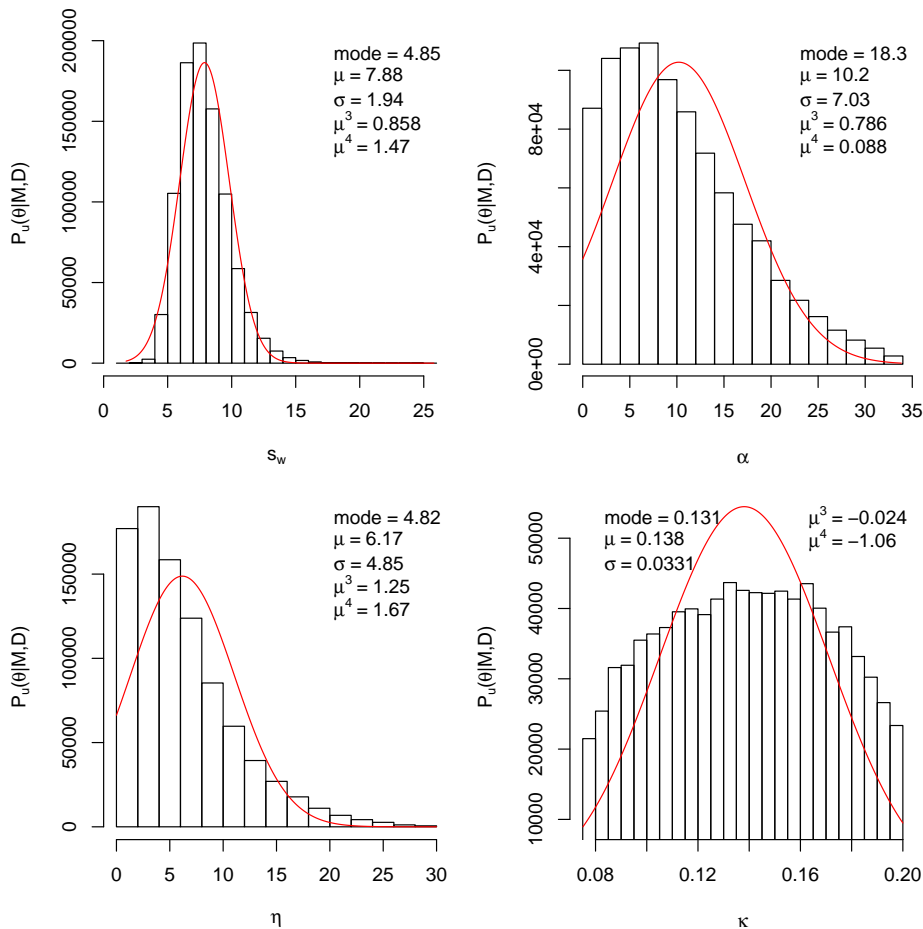
Figure 6. The unnormalised posterior distribution of s_w, α, η and κ of the LRJ1 model. The histograms are made with 90,5004 posterior samples of a cold chain. For each panel, the red curve shows the fit of Gaussian distribution to the unnormalised posterior density. The mode, mean (μ), standard deviation (σ), skewness (μ_3) and kurtosis (μ_4) are shown for each posterior distribution.

uneven sampling and/or correlated noise. Since RV variations have similar characteristics, our work may also provide insights for disentangling periodic signals from stochastic variability in quasar light curves (e.g. Graham et al. 2015; Vaughan et al. 2016).

In summary, the Goldilocks principle provides an approach to balance between overfitting and underfitting of noise by statistical models, which may poorly reflect the underlying physics and thus are unable to disentangle noise from signals. Although a Gaussian process framework has been proposed to partly account for the underlying physics (Rajpaul et al. 2015), the jitter may not be properly modeled due to the flexibility of Gaussian process models and the simplification of the complex relationship between RV variations and stellar activity indexes. Further studies on the statistical property of stellar activity proxies and their connection with RV variations are essential steps towards an astrophysically motivated modeling of stellar jitter. A probable method is the nonlinear time series analysis which connects the nonlinear dynamical system with the time series of some system outputs (Kantz & Schreiber 2004; Sugihara et al. 2012). This idea has inspired us to build the lagged $R_{\rm HK}$-dependent jitter model which performs well in our analyses. Moreover, correlated noise and deterministic signals can be well distinguished using surrogate time series, a concept developed in the community of nonlinear time series (Schreiber & Schmitz 2000). These facts justify further investigations into the nonlinear approach of modeling RV noise.

APPENDIX: KECK DATA OF GJ 445

REFERENCES

Akaike H., 1974, Automatic Control, IEEE Transactions on, 19, 716
Alvarez W., Muller R. A., 1984, Nat., 308, 718
Anglada-Escudé G. et al., 2013, Astronomy & Astrophysics, 556, A126
Bailer-Jones C. A. L., 2011, MNRAS, 416, 1163
Baluev R. V., 2013, Monthly Notices of the Royal Astronomical Society, 429, 2052
Batygin K., 2015, MNRAS, 451, 2589
Boffetta G., Carbone V., Giuliani P., Veltri P., Vulpiani A., 1999, Physical review letters, 83, 4662
Chib S., Jeliazkov I., 2001, Journal of the American Statistical Association, 96, 270

Table 5. The Keck measurements of GJ 445.

Julian Days	RV[m/s]	RV error[m/s]	R_{HK}
2450840.15414	1.82	2.52	0.7041
2450862.05138	-15.10	2.61	0.4365
2451171.11243	6.22	3.09	0.5667
2451173.15170	-6.46	2.70	0.5500
2451174.14020	3.09	2.91	0.7017
2451229.02528	-16.97	2.88	0.6536
2451312.83299	4.72	2.33	0.6772
2451581.05520	-0.05	2.72	0.6771
2451702.84804	5.85	2.61	0.5760
2451983.03906	-3.28	3.36	0.3824
2452333.05276	10.70	3.55	0.5765
2452654.07529	-2.00	2.94	0.3798
2452681.03126	11.68	3.64	0.4286
2453018.11966	7.61	2.76	0.3705
2453399.01632	0.80	2.87	0.6102
2454131.08186	7.17	3.03	0.6257
2454277.80190	-0.04	2.59	0.5708
2454278.82143	-3.37	2.88	0.5773
2454279.81260	-1.15	2.79	0.6036
2454285.83863	4.57	3.37	0.5528
2454294.86588	6.86	3.01	0.7721
2454304.84650	5.53	2.55	0.4551
2454305.85101	0.00	2.30	0.5399
2454306.84962	-4.73	2.59	0.6472
2454307.88909	-4.51	2.74	0.2917
2454308.86895	-6.74	3.57	0.3674
2454309.85157	-0.65	2.87	1.2438
2454310.84423	-2.85	2.76	0.5632
2454311.83910	-13.70	2.95	0.5975
2454312.83456	-4.73	2.87	0.9761
2454313.83837	1.69	2.89	0.5117
2454314.86490	-0.83	3.16	0.6875
2454455.14057	5.31	2.97	0.7055
2454455.14674	2.30	2.99	0.7308
2454491.04532	0.12	2.54	0.5859
2454546.04764	0.62	2.33	0.5356
2454600.95556	-0.47	2.74	0.6064
2454601.92483	-2.04	1.99	0.6463
2454701.74852	2.92	2.85	0.4183
2454701.75598	4.35	2.91	0.5082
2454702.74186	0.80	2.87	0.7380
2454702.74938	-1.07	3.21	0.5221
2454703.74693	4.92	2.61	0.3905
2454703.75477	-0.73	2.59	0.6241
2454704.73349	7.15	2.83	0.6441
2454704.74171	-0.16	3.44	0.4719
2454968.95856	-2.12	2.71	0.6697
2454968.96572	-0.99	3.23	0.4139
2455021.85243	-3.12	3.86	0.4572
2455049.79414	-4.34	3.01	0.6463
2455258.99615	-12.23	2.82	0.4616
2455313.90921	9.88	2.59	0.5754
2455371.79182	0.60	2.68	0.3061
2455637.04757	-3.31	2.43	0.5640
2455638.02685	1.23	2.56	0.4916
2455663.86110	0.46	2.30	0.6717
2455668.88064	10.32	2.40	0.6443
2455670.92034	6.46	2.45	0.6590
2455671.92802	5.80	2.60	0.7044
2455672.92840	4.46	2.45	0.7519
2455673.89382	6.65	2.63	0.6778
2455703.84580	-6.13	2.80	0.5339
2455704.76119	-5.27	2.78	0.5667
2455705.77066	-7.64	2.52	0.6797

Cumming A., 2004, Monthly Notices of the Royal Astronomical Society, 354, 1165

Díaz R. et al., 2016, Astronomy & Astrophysics, 585, A134

Dumusque X., Boisse I., Santos N., 2014, The Astrophysical Journal, 796, 132

Dumusque X. et al., 2012, Nature, 491, 207

Dumusque X., et al., 2016, in prep.

Feng F., Bailer-Jones C. A. L., 2013, ApJ, 768, 152

Feng F., Bailer-Jones C. A. L., 2014, MNRAS, 442, 3653

Feroz F., Hobson M. P., 2014, MNRAS, 437, 3540

Fischer D. et al., 2016, ArXiv e-prints

Ford E. B., Gregory P. C., 2007, in Astronomical Society of the Pacific Conference Series, Vol. 371, Statistical Challenges in Modern Astronomy IV, Babu G. J., Feigelson E. D., eds., p. 189

Foreman-Mackey D., Montet B. T., Hogg D. W., Morton T. D., Wang D., Schölkopf B., 2015, ApJ, 806, 215

Friel N., Wyse J., 2012, Statistica Neerlandica, 66, 288

Gelman A., Rubin D. B., 1992, Statistical science, 457

Graham M. J. et al., 2015, Nature, 518, 74

Gregory P., 2005, Bayesian Logical Data Analysis for the Physical Sciences: A Comparative Approach with Mathematica® Support. Cambridge University Press

Haario H., Saksman E., Tamminen J., 2001, Bernoulli, 223

Han C., Carlin B. P., 2011, Journal of the American Statistical Association

Hasselmann K., 1976, Tellus, 28, 473

Hays J. D., Imbrie J., Shackleton N. J., 1976, Science, 194, 1121

Hurvich C. M., Tsai C.-L., 1989, Biometrika, 76, 297

Kantz H., Schreiber T., 2004, Nonlinear time series analysis, Vol. 7. Cambridge university press

Kass R. E., Raftery A. E., 1995, Journal of the american statistical association, 90, 773

Kipping D. M., 2013, MNRAS, 434, L51

Liddle A. R., 2007, Monthly Notices of the Royal Astronomical Society: Letters, 377, L74

Mayor M. et al., 2003, The Messenger, 114, 20

Melott A. L., Bambach R. K., Petersen K. D., McArthur J. M., 2012, Journal of Geology, 120, 217

Milankovitch M., 1930, Mathematische Klimalehre und astronomische Theorie der Klimaschwankungen. Gebrueder Borntraeger

Mortier A. et al., 2016, A&A, 585, A135

Neves V. et al., 2012, A&A, 538, A25

O'Toole S. J., Tinney C. G., Jones H. R. A., Butler R. P., Marcy G. W., Carter B., Bailey J., 2009, MNRAS, 392, 641

Pelletier J. D., Turcotte D. L., 1997, Journal of Hydrology, 203, 198

Petrovay K., 2010, Living Reviews in Solar Physics, 7

Pojmanski G., 2002, Acta Astronomica, 52, 397

Rajpaul V., Aigrain S., Osborne M. A., Reece S., Roberts S., 2015, MNRAS, 452, 2269

Raup D. M., Sepkoski J. J., 1984, Proceedings of the National Academy of Science, 81, 801

Roberts G. O., Gelman A., Gilks W. R., et al., 1997, The annals of applied probability, 7, 110

Schreiber T., Schmitz A., 2000, Physica D: Nonlinear Phenomena, 142, 346

Schwarz G., et al., 1978, The annals of statistics, 6, 461

Spiegelhalter D. J., Best N. G., Carlin B. P., Van Der Linde A., 2002, Journal of the Royal Statistical Society: Series B (Statistical Methodology), 64, 583

Suárez Mascareño A., Rebolo R., González Hernández J. I., Esposito M., 2015, MNRAS, 452, 2745

Sugihara G., May R., Ye H., Hsieh C.-h., Deyle E., Fogarty M., Munch S., 2012, science, 338, 496

Takens F., 1981, Detecting strange attractors in turbulence. Springer

Tobias S., Weiss N., Kirk V., 1995, Monthly Notices of the Royal Astronomical Society, 273, 1150

Tuomi M., 2011, A&A, 528, L5

Tuomi M., 2012, A&A, 543, A52

Tuomi M., Anglada-Escudé G., 2013, Astronomy & Astrophysics, 556, A111

Tuomi M., Jenkins J. S., 2012, ArXiv e-prints

Tuomi M., Jones H. R. A., 2012, A&A, 544, A116

Tuomi M. et al., 2013, A&A, 551, A79

Tuomi M., et al., 2016, submitted

van Leeuwen F., 2007, A&A, 474, 653

Vanderburg A., Plavchan P., Johnson J. A., Ciardi D. R., Swift J., Kane S. R., 2016, ArXiv e-prints

Vaughan S., Uttley P., Markowitz A. G., Huppenkothen D., Middleton M. J., Alston W. N., Scargle J. D., Farr W. M., 2016, ArXiv e-prints

Vogt S., Crawford D., Craine E., et al., 1994, in Proc. SPIE, Vol. 2198, SPIE, p. 362

Vogt S. S., Butler R. P., Rivera E. J., Haghighipour N., Henry G. W., Williamson M. H., 2010, ApJ, 723, 954

von Toussaint U., 2011, Reviews of Modern Physics, 83, 943

Wunsch C., 2004, Quaternary Science Reviews, 23, 1001

Zechmeister M., Kürster M., Endl M., 2009, A&A, 505, 859